Japanese Journal of Applied Physics **56**, 030304 (2017) **RAPID COMMUNICATION**
https://doi.org/10.7567/JJAP.56.030304

# Inductively-coupled-plasma reactive ion etching of single-crystal $\beta$-$Ga_2O_3$

Liheng Zhang[1*], Amit Verma[2], Huili (Grace) Xing[1,2], and Debdeep Jena[1,2]

[1]*Department of Materials Science and Engineering, Cornell University, Ithaca, NY 14853, U.S.A.*
[2]*School of Electrical and Computer Engineering, Cornell University, Ithaca, NY 14853, U.S.A.*

*E-mail: lz388@cornell.edu

Received December 27, 2016; accepted January 11, 2017; published online February 9, 2017

Dry etching behavior of unintentionally-doped ($\bar{2}01$) $\beta$-$Ga_2O_3$ has been studied in a $BCl_3$/Ar chemistry using inductively-coupled-plasma reactive ion etching (ICP-RIE). The effects of various etch parameters like ICP and RIE powers, $BCl_3$/Ar gas ratio and chamber pressure on etch rate are studied systematically. Higher ICP, RIE powers and lower pressure conditions are found to enhance the etch rate. A synergic etching mechanism between chemical and physical components is proposed and used to obtain fast $Ga_2O_3$ etch rates more than 160 nm/min, nearly-vertical sidewalls and smooth etched surfaces. The findings of this work will enable $Ga_2O_3$ vertical devices for power electronics.


Wide bandgap semiconductors such as SiC and GaN are being pursued to replace Si in power electronic devices for the simultaneous miniaturization and improvements in the efficiency and system performance.[1–3] Recently, a new wide-bandgap semiconductor $\beta$-$Ga_2O_3$ has attracted much attention because of its potential to exceed both SiC and GaN in high-voltage devices.[4] $\beta$-$Ga_2O_3$ has a large bandgap $E_g$ (~4.5–4.9 eV) and high estimated breakdown field $F_{br}$ (~8 MV/cm).[4] Because of its superior material properties, its Baliga's figure of merit is four times or more larger than SiC or GaN, indicating that $Ga_2O_3$ has the potential to out-perform SiC and GaN power devices.[4] Moreover, bulk crystals of $Ga_2O_3$ have been recently grown by traditional melt grown methods such as Chochralski,[5,6] edge-defined, film fed (EFG) growth[7] and floating zone.[8,9] Consequently, high quality single crystal substrates of $\beta$-$Ga_2O_3$ of 4-in. diameter have become commercially available.[4] The availability of large area bulk crystals of $\beta$-$Ga_2O_3$ makes it economically competitive to other wide-bandgap semiconductor technologies currently being pursued for power electronics.

Device processing techniques for $Ga_2O_3$ are in their infancy. Lateral power devices such as metal–semiconductor field-effect transistors (MESFETs) and MOSFETs on $Ga_2O_3$ have been fabricated and have demonstrated good current modulation and high breakdown voltages.[10–14] Vertical devices are suitable for power electronics applications requiring very high voltage regulation; however, $Ga_2O_3$ vertical three-terminal power transistors have not yet been thoroughly studied. Two-terminal vertical Schottky diodes have been studied[4,15] and have recently demonstrated more than 1 kV breakdown voltage.[16] To develop three-terminal devices like vertical transistors, and for device isolation and electric field sculpting in vertical devices, it is critical to develop well-controlled precision etching processes that enables sharp profiles, minimum surface damage, and smooth etched surface morphologies.

Like GaN, $Ga_2O_3$ is also relatively chemically inert and has a high Ga–O bond strength (363.6 kJ/mol).[17] Wet etching of single crystal $Ga_2O_3$ has shown very low etch rates at room temperature.[18,19] Enhanced etch rates can be obtained with wet etching at elevated temperatures, however with slanted sidewalls.[19] Compared to wet etching, dry etching provides more controllable anisotropy and smaller feature sizes. Few studies have been done on the dry etching behavior of $Ga_2O_3$.[17,20,21] Liang et al. studied the effect of $SF_6$/Ar ratio on $Ga_2O_3$ etch rate and surface morphology using inductively-coupled plasma (ICP). They have found that $SF_6$ is the main etching species with Ar assisting to remove non-volatile etch products.[17] They also found that by tuning the $SF_6$/Ar ratio, surface damage could be minimized.[17] Zhou et al. etched $Ga_2O_3$ formed by oxidizing GaN using $NF_3$ and $Cl_2$/Ar by reactive ion etching (RIE) and found that $NF_3$ gives higher etch rate.[20] Hogan et al. compared RIE with ICP on the etch behavior of different crystal planes of $Ga_2O_3$ and found that ICP gives better surface morphology and higher etch rate using Cl-based chemistry.[21] They also found that $BCl_3$ is the main etchant in the $BCl_3/Cl_2$ mixture and that the (010) and ($\bar{2}01$) planes etch much faster than the (100) plane.[21]

In this work,[22] we use a $BCl_3$/Ar gas mixture in an ICP-RIE system to etch $Ga_2O_3$ because $BCl_3$ has been shown to etch $Ga_2O_3$ faster than $Cl_2$[21] and Ar gives an extra flexibility in tuning relative physical and chemical components. We use ICP to create a high-density plasma that is expected to increase the etch rate and yield smoother surface morphologies than pure RIE.[21] We adjust different parameters in ICP-RIE etching such as ICP power, RIE power, chamber pressure and $BCl_3$/Ar gas ratio to examine their effects on etch rate, surface morphology and etch profile. Etch rates exceeding ~160 nm/min with nearly-vertical sidewalls and smooth etched surfaces are obtained under the optimal etching conditions.

For the etching study, 2-in. unintentionally doped (UID; electron concentration ~$10^{17}$ $cm^{-3}$) $Ga_2O_3$ wafers of ($\bar{2}01$) surface orientation from Tamura Inc. were diced into 5 × 5 $mm^2$ pieces and cleaned in acetone and isopropanol (IPA) and blown dried with $N_2$. The samples were patterned with AZ S1813 photoresist (PR) using contact photolithography and a mask of various sizes of rectangular strips. The samples were then etched in a Plasma-Therm 770 ICP-RIE system that applies an RF power (ICP power) to a coil to inductively create a high-density plasma and a separate RF power (RIE power) on the chuck to direct the reactive ions to the substrate. To study the effect of each parameter (ICP power, RIE power, chamber pressure, and gas ratio), one parameter is varied within a reasonable range while other parameters are kept fixed. The etch rate was measured using a Tencor P-10 surface profilometer. Scanning electron microscopy (SEM) images were then taken at a 79° tilt angle to examine etch

 

profiles and atomic force microscopy (AFM) was used to measure the surface roughness.

Dry etching consists of both physical and chemical etch components. The physical component is from ions bombarding the sample surface. Pure physical etching is anisotropic and can cause severe surface damage and rough surface because of sputtering.[23)] Free radicals and ions form highly reactive species that can react with atoms on the sample surface, giving rise to a chemical component of etching. These chemical reactions take place preferably at active sites where there are defects.[23)] Pure chemical etching can therefore roughen the surface because of favored reactions and etch byproducts.[23)] A synergic mechanism between physical and chemical components usually results in a higher etch rate than each component working individually, because the chemical reaction can help break bonds while physical bombardment can create surface defects and remove etch byproducts to enhance the chemical reaction.[23)] Synergic etch has also been shown to result in smooth surface morphologies because the physical component can help remove etch product and level out protruded features formed by non-uniform chemical reaction.[17)] Therefore, if enhanced etch rate and reduced root-mean-square (RMS) roughness are simultaneously achieved, it is an indication of a synergic etch mechanism. In the $BCl_3$/Ar mixture used in this study, the physical component of etching is from $Ar^+$ and $BCl_3$ derived ions bombarding the substrate surface, while Cl free radicals and other highly reactive species from $BCl_3$ react with atoms on the $Ga_2O_3$ surface to provide the chemical component of the etching process.

In the first set of experiments, RIE and ICP powers were varied while keeping the $BCl_3$/Ar gas flows at 35/5 sccm and chamber pressure during etch at 5 mTorr (Fig. 1). As shown in Fig. 1(a), at high ICP powers (900 W), the etch rate increases significantly with increasing RIE power, indicating that the physical component plays an important role because enhanced ion bombardment can help to remove etch products and simultaneously create surface defects to promote chemical reaction. However, at lower ICP power (350 W), the etch rate stays almost constant with increasing RIE power. This is possibly because at low ICP powers, not many Cl radicals are generated in the plasma and the chemical component is therefore weak. Therefore, an enhanced physical component does not go hand-in-hand with an as-strong chemical one. Moreover, as ICP power increases, the degree to which the etch rate increases with RIE power also increases. At 550 W ICP power, the etch rate increases from 72.6 to 93.5 nm/min (~28% increase) whereas the etch rate increases from 94 to 165 nm/min at 900 W ICP power (~75% increase). For the RIE power of 60 W, the $Ga_2O_3$ etch rate increases almost linearly with increasing ICP power as shown in Fig. 1(b). This happens because increasing ICP power will generate more reactive species and positive ions in the plasma, which will enhance both chemical and physical components. By using ICP-RIE etching at high ICP powers, we have obtained ~4× enhancement in the etching rates compared to earlier dry etching studies performed on $\beta$-$Ga_2O_3$.[17,20,21)]

After studying the effect of ICP and RIE powers, we studied the effect of the $BCl_3$/Ar gas ratio on $Ga_2O_3$ etch rate. Experiments at following $BCl_3$/Ar gas flow rates were carried out: 40/0, 35/5, 25/15, 20/20, 15/20 sccm, keeping the total gas flow rate at 40 sccm. ICP and RIE powers of 900 W and 30 W were used for these studies while keeping the chamber pressure at 5 mTorr. The measured etch rates for different gas flow rates are shown in Fig. 2. We find that adding Ar to $BCl_3$ does not change the etch rate significantly till a $BCl_3$/Ar flow rate of 25/15 sccm. Further increase in the Ar flow rate decreases the etch rate. Ar is expected to promote physical etching because $Ar^+$ ions can help remove etch products and creating active sites for chemical etching. If $BCl_3$ only provides chemical component by producing the

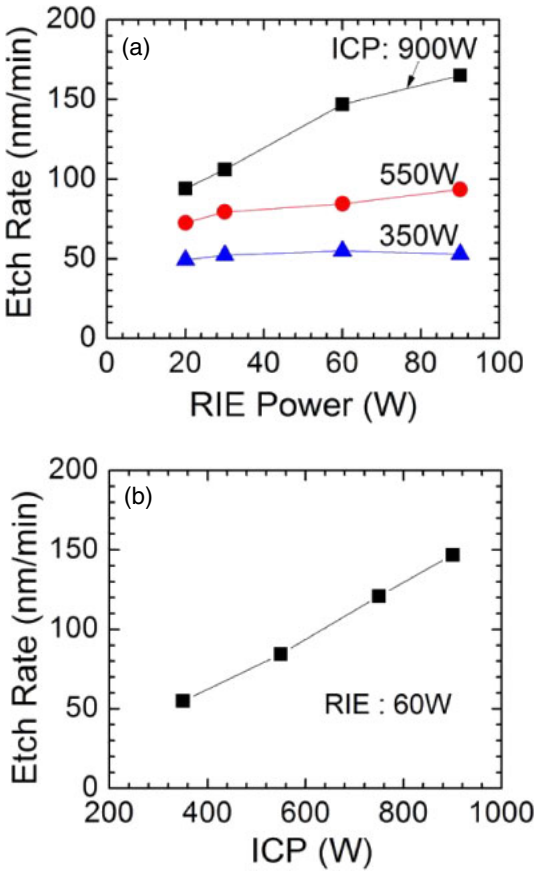


**Fig. 1.** (Color online) (a) Etch rate of UID ($\bar{2}01$) $\beta$-$Ga_2O_3$ vs RIE power at various ICP powers. (b) Etch rate vs ICP power at 60 W RIE power. All etches have been performed at 5 mTorr chamber pressure and $BCl_3$/Ar flow rates of 35/5 sccm.

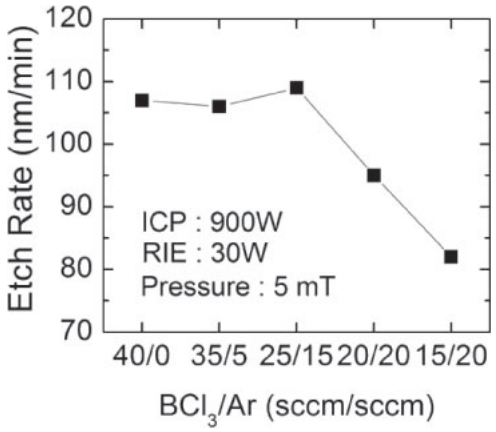


**Fig. 2.** Etch rate of UID ($\bar{2}01$) $\beta$-$Ga_2O_3$ vs $BCl_3$/Ar flow rate at 5 mTorr chamber pressure, 30 W RIE and 900 W ICP powers.

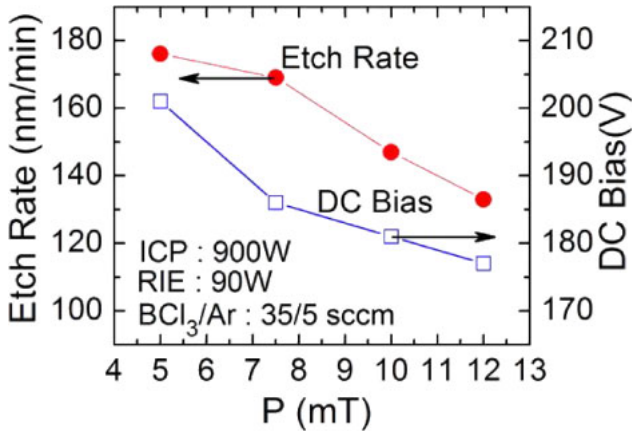


**Fig. 3.** (Color online) Etch rate (left-axis) of UID ($\bar{2}01$) $\beta$-$Ga_2O_3$ and DC bias voltage (right-axis) vs chamber pressure at 900 W ICP, 90 W RIE, and 35/5 sccm $BCl_3$/Ar flow rate.

reactive Cl radical, adding Ar to pure $BCl_3$ would enhance etch rate because of synergic mechanism. A previous study found that $BCl_3$ produces heavy $BCl^{+2}$ and $BCl^{+3}$ ions that do physical etching as well.[24] Therefore, $BCl_3$ by itself can provide both chemical and physical etch components in the plasma to promote the synergic mechanism. As more Ar is added, the etch rate eventually drops because of the lack of Cl radical. The etch rate in pure Ar was not obtained because the plasma could not be lit at same ICP/RIE powers and pressure. However, following the trend in Fig. 2, further reduction in the etch rate is expected for pure Ar. Liang et al. have performed a similar study of $Ga_2O_3$ etching with a $SF_6$/Ar mixture that shows a trend similar to Fig. 2 and negligible etch rate with pure Ar.[17]

In the last set of experiments, we studied the effect of chamber pressure on ($\bar{2}01$) $\beta$-$Ga_2O_3$ etch rate while the ICP/RIE powers are kept at 900 W/90 W and $BCl_3$/Ar flow rate at 35/5 sccm. As shown in Fig. 3, the etch rate decreases when the chamber pressure increases from 5 to 12 mTorr. At higher pressures, more collisions occur between particles leading to a reduced mean-free path and recombination of free radicals. This enhanced recombination leads to less chemically reactive species and reduced chemical component of etching.[23] Further, the reduced DC bias across the sheath at higher pressures reduces ion bombardment energies and therefore the physical component. Reduction in both physical and chemical components leads to the decrease in etch rate at higher chamber pressures.

The morphology of the sample surface before and after etching is studied using AFM. The RMS roughness is compared across different etching conditions mentioned in previous paragraphs. The effect of increasing RIE power on the RMS roughness is shown in Fig. 4(a). With increasing RIE power, the etched surface maintains roughly the same roughness as the unetched surface, suggesting that the etching has caused minimal surface damage. The RMS roughness even decreases slightly as the RIE power increases beyond 60 W, indicating that a balance is reached between the physical and chemical etching components. This reduced RMS at higher RIE is consistent with the enhanced etch rate at higher RIE, both being evidences for synergic mechanism.

Figure 4(b) shows the influence of the $BCl_3$/Ar flow rate on sample roughness. When $BCl_3$ flow rate is greater than or

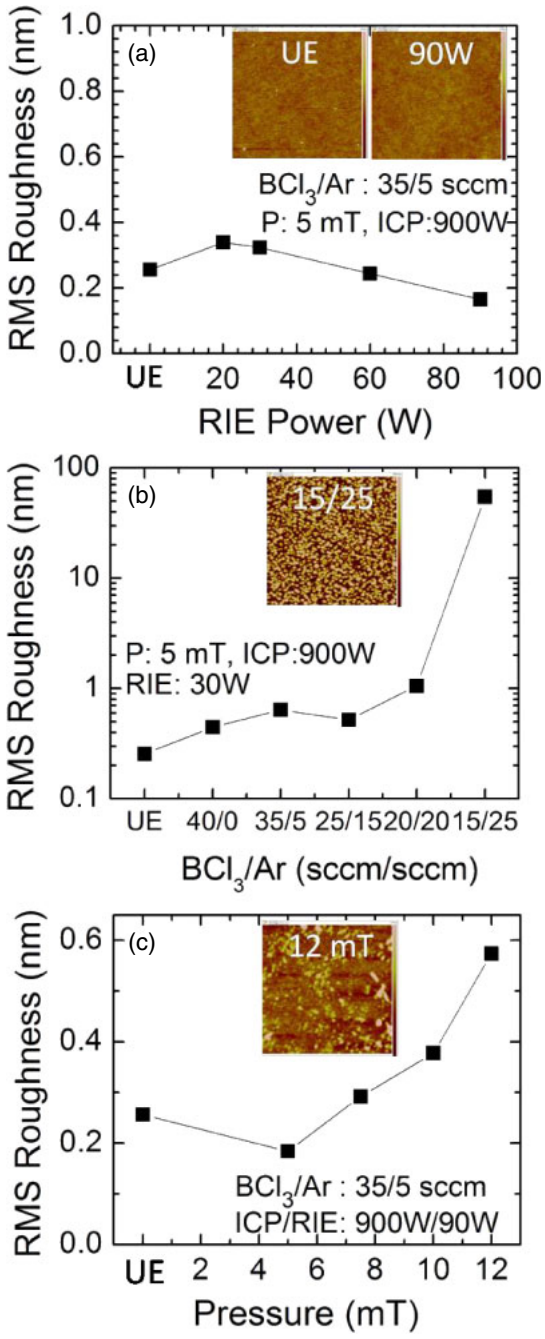


**Fig. 4.** (Color online) (a) RMS roughness of unetched (UE) UID ($\bar{2}01$) $\beta$-$Ga_2O_3$ sample and samples etched under different RIE powers (inset: AFM image of UE and 90 W RIE sample, height scale bar: ±2 nm, scan size: 5 × 5 μm$^2$), (b) RMS roughness for UE sample and samples etched with different $BCl_3$/Ar gas flows (inset: AFM image of $BCl_3$/Ar 15/25 sccm sample, height scale bar: ±100 nm, scan size: 5 × 5 μm$^2$), (c) RMS roughness for UE sample and samples etched at different chamber pressures (inset: AFM image of 12 mTorr sample, height scale bar: ±2 nm, scan size: 5 × 5 μm$^2$).

equal to Ar flow rate, the RMS roughness does not change much from the unetched sample (RMS: 0.256 nm), indicating synergic etching. However, for $BCl_3$/Ar flow rate of 15/25 sccm, RMS roughness increases drastically to 54.8 nm. This abrupt increase in roughness is probably because there are not enough Cl radicals in this condition to do chemical etching and the physical and chemical etch components go out of balance. Pure $BCl_3$ results in an RMS as good as the mixture of $BCl_3$ and Ar, confirming that $BCl_3$ provides $BCl^{+2}$ and

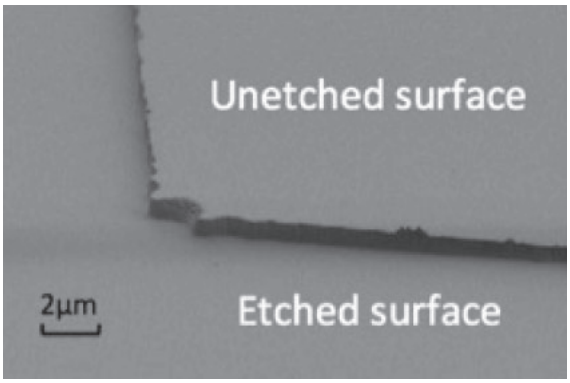


**Fig. 5.** SEM image of etched $Ga_2O_3$ showing vertical sidewalls and smooth etched surface (ICP/RIE 900 W/60 W, chamber pressure 5 mTorr, $BCl_3$/Ar 35/5 sccm).

$BCl^{+3}$ ions that also perform physical etching. This is consistent with the etch rate data shown in Fig. 2 that shows that pure $BCl_3$ etches as fast as $BCl_3$/Ar mixture.

The RMS roughness increases only slightly with increase of chamber pressure as shown in Fig. 4(c), suggesting that synergic etch mechanism is maintained in the 5–12 mTorr chamber pressure range. From these studies, we identify a large window of ICP-RIE etching conditions under which very smooth surface morphologies with sub 1 nm RMS roughness for $5 \times 5\,\mu m^2$ scans can be obtained. This finding will be crucial for device fabrication, if can be combined with sharp etched sidewalls.

SEM images were taken at a tilt angle of 79° to examine the etch profile and sidewalls of the $(\bar{2}01)$ $\beta$-$Ga_2O_3$ under all etch conditions. Smooth and nearly vertical sidewalls were obtained for the samples etched under the synergic mechanism. Figure 5 shows the SEM image of the sample etched at 350 W/60 W ICP/RIE, 5 mTorr chamber pressure and 35/5 sccm $BCl_3$/Ar flow rate. Because physical etching is anisotropic and chemical etching is isotropic,[23)] the synergic etching occurs only on the surface of substrate and chemical etching on the sidewalls. Because synergic etching is much faster than chemical etching acting alone,[23)] etching in the vertical direction dominates and creates vertical sidewalls.

To summarize this work, we have systematically studied the effects of various etch parameters on etch rate, surface morphology and etch profile of $\beta$-$Ga_2O_3$. RIE, ICP powers, chamber pressure and gas mixture ratio are shown to have prominent impacts on the etch rate. A synergic etching mechanism between chemical and physical components is confirmed. This mechanism can provide higher etch rates and smoother surfaces than either chemical or physical component acting individually. The etch parameters have been shown to be tunable to balance physical and chemical components to achieve smooth surface and nearly vertical profile. These findings are important for the processing of vertical power devices with high performance.

**Acknowledgments** This work was supported by the NSF DMREF program (Award Number 1534303) and made use of the Cornell NanoScale Science and Technology Facility (CNF) which is supported through the NSF NNCI program (Grant Number ECCS-1542081).

1) J. L. Hudgins, G. S. Simin, E. Santi, and M. A. Khan, IEEE Trans. Power Electron. **18**, 907 (2003).
2) D. A. Marckx, Subcontract Rep. NREL/SR-500-38515 (2006).
3) B. J. Baliga, Semicond. Sci. Technol. **28**, 074011 (2013).
4) M. Higashiwaki, K. Sasaki, H. Murakami, Y. Kumagai, A. Koukitu, A. Kuramata, T. Masui, and S. Yamakoshi, Semicond. Sci. Technol. **31**, 034001 (2016).
5) Z. Galazka, R. Uecker, K. Irmscher, M. Albrecht, D. Klimm, M. Pietsch, M. Brutzam, R. Bertram, S. Ganschow, and R. Fornari, Cryst. Res. Technol. **45**, 1229 (2010).
6) Z. Galazka, R. Uecker, D. Klimm, K. Irmscher, M. Naumann, M. Pietsch, A. Kwasniewski, R. Bertram, S. Ganschow, and M. Bickermann, ECS J. Solid State Sci. Technol. **6**, Q3007 (2017).
7) H. Aida, K. Nishiguchi, H. Takeda, N. Aota, K. Sunakawa, and Y. Yaguchi, Jpn. J. Appl. Phys. **47**, 8506 (2008).
8) N. Ueda, H. Hosono, R. Waseda, and H. Kawazoe, Appl. Phys. Lett. **70**, 3561 (1997).
9) E. G. Víllora, K. Shimamura, Y. Yoshikawa, K. Aoki, and N. Ichinose, J. Cryst. Growth **270**, 420 (2004).
10) M. Higashiwaki, K. Sasaki, A. Kuramata, T. Masui, and S. Yamakoshi, Appl. Phys. Lett. **100**, 013504 (2012).
11) M. Higashiwaki, K. Sasaki, T. Kamimura, M. H. Wong, D. Krishnamurthy, A. Karamata, T. Masui, and K. Yamakoshi, Appl. Phys. Lett. **103**, 123511 (2013).
12) W. S. Hwang, A. Verma, H. Peelaers, V. Protasenko, S. Rouvimov, H. Xing, A. Seabaugh, W. Haensch, C. V. de Walle, Z. Galazka, M. Albrecht, R. Fornari, and D. Jena, Appl. Phys. Lett. **104**, 203111 (2014).
13) M. H. Wong, K. Sasaki, A. Kuramata, S. Yamakoshi, and M. Higashiwaki, IEEE Electron Device Lett. **37**, 212 (2016).
14) A. J. Green, K. D. Chabak, E. R. Heller, R. C. Fitch, Jr., M. Baldini, A. Fielder, K. Irmscher, G. Wagner, Z. Galazka, S. E. Tetlak, A. Crespo, K. Leedy, and G. H. Jessen, IEEE Electron Device Lett. **37**, 902 (2016).
15) K. Sasaki, M. Higashiwaki, A. Kuramata, T. Masui, and S. Yamakoshi, IEEE Electron Device Lett. **34**, 493 (2013).
16) K. Konishi, K. Goto, Q. T. Thieu, R. Togashi, H. Murakami, Y. Kumagai, B. Monemar, A. Kuramata, S. Yamakoshi, and M. Higashiwaki, presented at Device Research Conf., 2016.
17) H. Liang, Y. Chen, X. Xia, C. Zhang, R. Shen, Y. Liu, Y. Luo, and G. Du, Mater. Sci. Semicond. Process. **39**, 582 (2015).
18) S. Ohira and N. Arai, Phys. Status Solidi C **5**, 3116 (2008).
19) T. Oshima, T. Okuno, N. Arai, Y. Kobayashi, and S. Fujita, Jpn. J. Appl. Phys. **48**, 040208 (2009).
20) Y. Zhou, C. Ahyi, T. Isaacs-Smith, M. Bozack, C. Tin, J. Williams, M. Park, A. Cheng, J. Park, D. Kim, D. Wang, E. A. Preble, A. Hanser, and K. Evans, Solid-State Electron. **52**, 756 (2008).
21) J. E. Hogan, S. W. Kaun, E. Ahmadi, Y. Oshima, and J. S. Speck, Semicond. Sci. Technol. **31**, 065006 (2016).
22) L. Zhang, A. Verma, H. G. Xing, and D. Jena, 23rd Int. Workshop Oxide Electronics, 2016, p. 159.
23) J. D. Plummer, M. Deal, and P. B. Griffin, *Silicon VLSI Technology: Fundamentals, Practice, and Modeling* (Prentice-Hall, Upper Saddle River, NJ, 2000) 1st ed., Chap. 10.
24) D. S. Rawal, H. K. Malik, V. R. Agarwal, A. K. Kapoor, B. K. Sehgal, and R. Muralidharan, IEEE Trans. Plasma Sci. **40**, 2211 (2012).